# High Antiferromagnetic Domain Wall Velocity Induced by Néel Spin-Orbit Torques

O. Gomonay,[1,2,*] T. Jungwirth,[3,4] and J. Sinova[1,3]
[1]*Institut für Physik, Johannes Gutenberg Universität Mainz, D-55099 Mainz, Germany*
[2]*National Technical University of Ukraine "KPI", 03056 Kyiv, Ukraine*
[3]*Institute of Physics Academy of Sciences of the Czech Republic, Cukrovarnicka 10, 162 00 Praha 6, Czech Republic*
[4]*School of Physics and Astronomy, University of Nottingham, Nottingham NG7 2RD, United Kingdom*
(Received 24 February 2016; revised manuscript received 21 May 2016; published 29 June 2016)

We demonstrate the possibility to drive an antiferromagnetic domain wall at high velocities by fieldlike Néel spin-orbit torques. Such torques arise from current-induced local fields that alternate their orientation on each sublattice of the antiferromagnet and whose orientation depends primarily on the current direction, giving them their fieldlike character. The domain wall velocities that can be achieved by this mechanism are 2 orders of magnitude greater than the ones in ferromagnets. This arises from the efficiency of the staggered spin-orbit fields to couple to the order parameter and from the exchange-enhanced phenomena in antiferromagnetic texture dynamics, which leads to a low domain wall effective mass and the absence of a Walker breakdown limit. In addition, because of its nature, the staggered spin-orbit field can lift the degeneracy between two 180° rotated states in a collinear antiferromagnet, and it provides a force that can move such walls and control the switching of the states.

DOI: 10.1103/PhysRevLett.117.017202

Antiferromagnets (AFs) are promising materials for spintronics because they show fast magnetic dynamics and low susceptibility to magnetic fields, and they produce no stray fields. These advantages stem from the antiferromagnetic ordering which consists of alternating magnetic moments on individual atomic sites with zero net magnetization, and whose orientation is described by the Néel vector. This also means that an AF cannot be efficiently manipulated by external magnetic fields, a fact that has relegated AFs as primarily passive elements in today's technology. The emerging field of antiferromagnetic spintronics focuses on reversing this trend, making AFs active elements in spintronic devices [1–4].

A new way to manipulate the Néel order parameter is the recently proposed relativistic Néel spin-orbit torque (NSOT) [5]. The NSOT is the antiferromagnetic version of the inverse spin-galvanic (Edelstein) mechanism [6–9], which generates current-induced spin-orbit torques in ferromagnets (FMs) [10,11]. It locally produces a nonequilibrium spin polarization in particular crystal structures that is proportional to the applied uniform current and alternates in sign between the different magnetic sublattices. The local nonequilibrium spin polarization results in a staggered spin-orbit field that couples effectively to the Néel order parameter, as shown in Fig. 1(a) [3,5,12].

The NSOT arises in crystals whose magnetic atoms have a local environment with broken inversion symmetry and where the two magnetic sublattices form inversion partners, such as in $Mn_2Au$ and CuMnAs. Its first observation has recently been reported in CuMnAs [3], with the measurements indicating that the NSOT switching involved a reconfiguration of a multiple-domain state of the AF. This motivates a study of current-induced AF dynamics beyond the coherent single-domain regime, in particular, a study of the antiferromagnetic domain wall (AFDW) motion driven by the fieldlike NSOT. Both 90° and 180° AFDWs are experimentally relevant since, in thicker CuMnAs films, an in-plane biaxial anisotropy dominates [3], while thinner films (below ∼10 nm) are uniaxial [13].

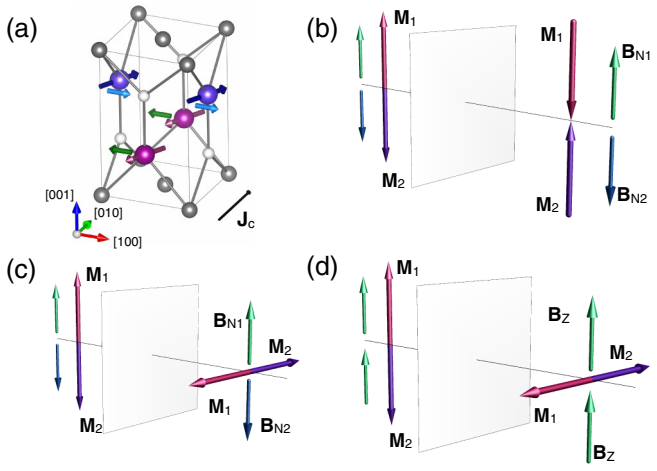


FIG. 1. (a) Crystal structure of AF CuMnAs. The two spin sublattices of the Mn atoms are $\mathbf{M}_{1/2}$ (red and purple). The current-induced staggered NSOT field ($\mathbf{B}_{N1/N2}$—green and blue) has an opposite sign at each Mn sublattice. The nonmagnetic As atoms (light grey) provide the locally broken inversion symmetry at the Mn inversion partner sites. $\mathbf{J}_c$ represents the current. (b) AFDW between 180° rotated AF domains in the presence of the staggered NSOT field. The energy density has opposite sign in the left and right domains, producing a ponderomotive force. (c,d) AFDW between 90° rotated AF domains in (c) the staggered NSOT field and (d) the uniform Zeeman ($\mathbf{B}_Z$) field.

 

In these crystals the staggered spin-orbit field is generated by an electrical current applied in the (001) plane. The NSOT field is oriented in the plane in the direction perpendicular to the current, and its amplitude from *ab initio* calculations is in the range of ~1–10 mT per $10^7$ A/cm$^2$.

In this Letter we present a theoretical study demonstrating that AFDWs can be controlled electrically by the fieldlike NSOTs with high efficiency. Moreover, the staggered NSOT field opens an unprecedented possibility to set into motion a 180° AFDW in a collinear AF. In addition, whereas the velocity of a ferromagnetic domain wall (FMDW) is limited by the Walker breakdown, in an AF only the much higher magnon velocity sets the upper limit [14–16]. In a FM the Walker breakdown arises when the FMDW begins to oscillate between a Bloch and Néel type driven by the competition of the external field torque and the internal anisotropy torque, which can be of similar order, as shown in Figs. 2(a) and 2(c). In an AF, on the other hand, the internal torque due to exchange is several orders of magnitude larger than any driving torque, which leads to a stiff AFDW, a very low effective mass of the AFDW, and no Walker-breakdown point, as shown in Figs. 2(a) and 2(b). At fields below the Walker breakdown, both the FM and AF have a similar dependence on the driving field. In our calculations (assuming no extrinsic pinning) we show that the velocities are proportional to the Néel field, and we estimate that they can reach values of ~10–100 km/s, orders of magnitude higher than in FMs. Also, by comparing the steady motion of a 90° AFDW in the presence of a uniform Zeeman field and the staggered spin-orbit field, we show that the velocities induced by the latter are much greater.

Experimentally, the AFDW can be dragged by a STM tip that generates a spin-polarized current, with the velocity of the AFDW equal to the velocity of the tip [17]. The AFDW can also be pushed by circularly polarized magnons [16]. In systems formed by antiferromagnetically coupled thin-film FMs (synthetic AFs), where the antiferromagnetic coupling is not as strong as in our case of bulk AF, an antiferromagnetic texture can be moved by the electric current due to dissipative (antidamping-like) spin torques [18–20]. Another proposed method to manipulate an AFDW is with the gradient of an external magnetic field [21]. None of these proposed methods for AFDW can reach the high velocities and efficiencies afforded by the fieldlike NSOT.

We consider a compensated collinear AF described by the sublattice magnetization vectors $\mathbf{M}_1$ and $\mathbf{M}_2$ ($|\mathbf{M}_1| = |\mathbf{M}_2| = M_s/2$), in which the electrical current generates the nonequilibrium staggered spin-orbit field described by vectors $\mathbf{B}_{\mathrm{N1}}$ and $\mathbf{B}_{\mathrm{N2}}$ acting on $\mathbf{M}_1$ and $\mathbf{M}_2$, respectively, as shown in Fig. 1(a). For convenience, we measure $\mathbf{B}_{\mathrm{N1/N2}}$ in units of the magnetic field. (The conversion to current density can be calculated by microscopic techniques [5]).

Due to the direct coupling between the atomic spins and the local fields, the current-induced contribution to the magnetic energy density of an AF takes the form $w = -\mathbf{M}_1 \cdot \mathbf{B}_{\mathrm{N1}} - \mathbf{M}_2 \cdot \mathbf{B}_{\mathrm{N2}} = -\mathbf{L} \cdot \mathbf{B}_{\mathrm{Neel}}$, where $\mathbf{L} \equiv \mathbf{M}_1 - \mathbf{M}_2$ is the Néel order parameter vector, and $\mathbf{B}_{\mathrm{Neel}} \equiv (\mathbf{B}_{\mathrm{N1}} - \mathbf{B}_{\mathrm{N2}})/2$. The sign and orientation of $\mathbf{B}_{\mathrm{Neel}}$ are determined by the sign and orientation of the electrical current. In the presence of an external uniform magnetic field or in a general case when $(\mathbf{B}_{\mathrm{N1}} + \mathbf{B}_{\mathrm{N2}})/2 \neq 0$, there is an additional uniform Zeeman field contribution, $\mathbf{B}_{\mathrm{Zee}}$, which in the magnetic energy density expression couples to the uncompensated magnetization of the AF, $\mathbf{M}_{\mathrm{AF}} = \mathbf{M}_1 + \mathbf{M}_2$. Zeeman and Néel fields act on an AF in different ways. The Néel field can change only the equilibrium orientation of the AF vector $\mathbf{L}$. On the other hand, the Zeeman field produces a small magnetization $\mathbf{M}_{\mathrm{AF}} = \mathbf{L} \times \mathbf{B}_{\mathrm{Zee}} \times \mathbf{L}/(M_s H_{\mathrm{ex}})$, where $H_{\mathrm{ex}}$ stands for the exchange field that keeps magnetic sublattices antiparallel.

The final expression for the magnetic energy density can then be written as

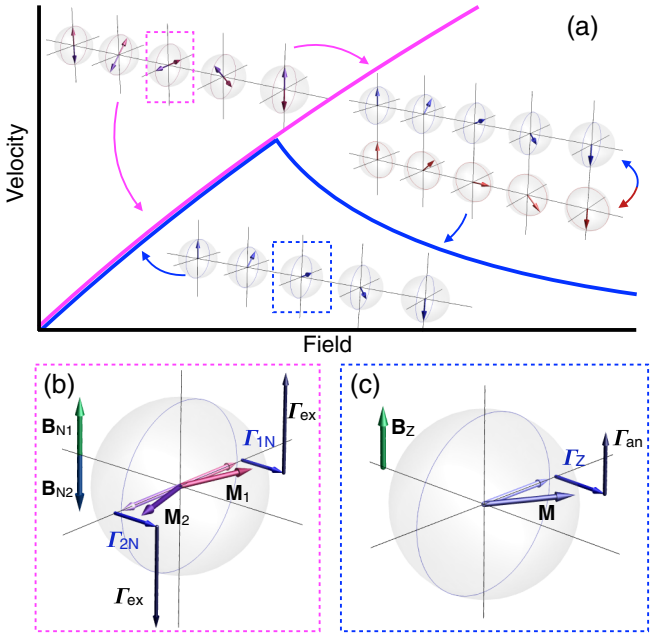


FIG. 2. (a) Schematic of Bloch domain wall velocity vs field for an AF (magenta line) and a FM (blue line). At low fields both FM and AF have the same velocity vs field, but beyond the Walker breakdown, the FM slows down as the domain wall character oscillates between Bloch and Néel. (b,c) Illustration of torques exerted on the AFDW and FMDW center. (b) The Néel field generates a torque ($\Gamma_{1N/2N}$) that cants $\mathbf{M}_{1/2}$ forward, and the much larger internal torque from the exchange interaction ($\Gamma_{\mathrm{ex}}$) rotates the sublattice magnetizations towards their respective easy axis directions, which causes the AFDW motion. $\Gamma_{\mathrm{ex}}/\Gamma_{1N/2N} \gg 1$ leads to a small deformation of the DW from its equilibrium (Bloch) configuration, i.e., to a very small AFDW mass. (c) In a FM the external driving field torque can reach a similar magnitude as the internal anisotropy torque ($\Gamma_{\mathrm{an}}$), leading to larger deformation of the FMDW, i.e., to a much larger FMDW mass.

$$w = -\frac{1}{2M_s H_{\rm ex}}(\mathbf{L}\times\mathbf{B}_{\rm Zee})^2 - \mathbf{L}\cdot\mathbf{B}_{\rm Neel}. \quad (1)$$

Equation (1) shows that the effect produced in AFs by the Zeeman field is (i) quadratic in $\mathbf{B}_{\rm Zee}$ and (ii) weakened due to the strong exchange interaction. In contrast, the effect of the Néel field is linear in $\mathbf{B}_{\rm Neel}$ and not diminished by the strong exchange interaction. Hence, its effect is much stronger. We also emphasize that the Néel field can remove the degeneracy of states with opposite direction of $\mathbf{L}$, while other physical fields can distinguish only between states with different orientations of $\mathbf{L}$. This directly implies that the Néel field can produce an effective force per area $2\mathbf{L}\cdot\mathbf{B}_{\rm Neel}$ that will set into motion the AFDW between 180° rotated domains, independent of the microscopic structure of the AFDW. The sign of $\mathbf{B}_{\rm Neel}$ (of the applied electrical current) determines the direction of the AFDW motion.

To study this problem in more detail, we consider a one-dimensional texture in a uniaxial AF in the presence of a Néel field parallel to the AF easy axis [see Fig. 1(b)]. Such an AF has two states that are magnetically equivalent at zero field with $\mathbf{L}_1 = -\mathbf{L}_2$ parallel to the easy axis. Both states have the same Zeeman energy, since $(\mathbf{L}_1\times\mathbf{B}_{\rm Zee})^2 = (\mathbf{L}_2\times\mathbf{B}_{\rm Zee})^2$, and therefore the Zeeman field can be neglected. The dynamics of an AF texture is described by phenomenological equations for the AF vector (see, e.g., Refs. [22–24]). In our case these equations are reduced to the following equation for the angle $\theta(x,t)$ between $\mathbf{L}$ and the easy axis:

$$c^2\frac{\partial^2\theta}{\partial x^2} - \ddot{\theta} - \gamma^2 H_{\rm ex}H_{\rm an}\sin\theta\cos\theta = \alpha_G\gamma H_{\rm ex}\dot{\theta} + \gamma^2 H_{\rm ex}B_{\rm Neel}\sin\theta, \quad (2)$$

where $\gamma$ is the gyromagnetic ratio, $H_{\rm an}$ is the magnetic anisotropy field, $c$ is the magnon velocity, and $\alpha_G$ is the Gilbert damping parameter.

Equation (2) has a solution which describes a moving AFDW separating domains with $\theta_1 = 0$ and $\theta_2 = \pi$. The velocity of steady motion,

$$v^{\rm AF}_{\rm steady} = \frac{2B_{\rm Neel}c}{\sqrt{\alpha_G^2 H_{\rm an}H_{\rm ex} + 4B^2_{\rm Neel}}}, \quad (3)$$

is obtained from the balance between the force produced by the Néel field and the internal (Gilbert) damping. In contrast to the FM case, the velocity is only limited by the magnon velocity $c = \gamma\sqrt{AH_{\rm ex}/M_s}$, where $A$ is the exchange stiffness [14–16].

We compare this result with the steady motion of the FMDW, separating 180° rotated domains in a uniaxial FM, induced by a Zeeman magnetic field or, equivalently, by the fieldlike component of a current-induced spin torque [25]. Such a FMDW cannot move while keeping its form since a parallel shift is connected with a variation of the total magnetization [15]. In contrast, the magnetization of an AF in the presence of the Néel field has a pure dynamic origin. Hence, the parallel shift of an AFDW does not affect the magnetization of the texture.

Steady motion of the FMDW in a uniaxial FM is often combined with the rotation of the magnetization around the easy axis with a constant angular velocity $\omega = \gamma B_{\rm Zee}/(1+\alpha_G^2)$. In this case the velocity of the steady motion is proportional to the damping coefficient: $v = \gamma\alpha_G x_{\rm DW}B_{\rm Zee}/(1+\alpha_G^2)$, where $x_{\rm DW} = \sqrt{A/H_{\rm an}M_s}$ is the wall width. In the more realistic case considered by Walker [26], the magnetic anisotropy function includes demagnetization energy. In this case magnetization in the moving FMDW makes a constant angle $\sin 2\varphi_0 = H_{\rm Zee}/H_c$ with the FMDW plane, where the critical field $H_c \approx \alpha_G H_{\rm dip-an}$ sets the Walker limit for the FMDW velocity (we assume that the dipolar anisotropy field $H_{\rm dip-an}$ is comparable to $H_{\rm an}$):

$$v^{\rm FM}_{\rm steady} = \frac{\gamma B_{\rm Zee}x_{\rm DW}}{\alpha_G\sqrt{1+\frac{H_{\rm dip-an}}{H_{\rm an}} - \left(\frac{H_{\rm dip-an}}{H_{\rm an}}\right)\sqrt{1-\frac{B^2_{\rm Zee}}{H_c^2}}}}. \quad (4)$$

The mobilities of AFDWs and of FMDWs below the Walker limit could be of the same order for systems with similar values of the wall width and Gilbert damping. This can be seen by comparing Eqs. (3) and (4):

$$\mu^{\rm FM} \equiv \frac{dv^{\rm FM}_{\rm steady}}{dB_{\rm Zee}} = \frac{\gamma x_{\rm DW}}{\alpha_G}, \quad (5)$$

$$\mu^{\rm AF} \equiv \frac{dv^{\rm AF}_{\rm steady}}{dB_{\rm Neel}} = \frac{c}{\alpha_G\sqrt{H_{\rm an}H_{\rm ex}}} \approx \frac{\gamma x_{\rm DW}}{\alpha_G}. \quad (6)$$

However, the limiting velocity of the AFDW coincides with the magnon velocity, $v^{\rm AF}_{\rm lim} = \gamma\sqrt{H_{\rm ex}A/M_s}$, which due to strong exchange enhancement, is much larger than the typical magnon velocity in a FM. On the other hand, in a FM the limiting (Walker) velocity $v^{\rm FM}_{\rm lim} \approx \gamma\sqrt{H_{\rm dip-an}A/M_s}$, where we have assumed $H_{\rm dip-an}$ is of the order of $H_{\rm an}$. Hence, $v^{\rm FM}_{\rm lim}$ is much smaller than $v^{\rm AF}_{\rm lim}$. For example, typical values of $v^{\rm AF}_{\rm lim} = c$ vary from 36 km/s in dielectric NiO [27], 40–50 km/s in metallic $\gamma - {\rm Mn}_{1-x}{\rm Cu}_x$ alloys [28–30], and up to 90 km/s for an AF $KFeS_2$ with extremely large magnon frequency (10 THz) [31]. For comparison, the highest FMDW velocities range from 100 m/s [32] to 400 m/s [33], and a velocity up to 750 m/s was recently achieved in a synthetic AF [20].

In order to illustrate the efficiency of the NSOT, we next compare the effects of the Néel and Zeeman fields on AFDWs. To do so, we reduce the complexity of Eq. (2), which fully describes the dynamics of the AF texture in all space, to one where the AFDW can be treated as a point

particle with an effective mass. This will be the case if, e.g., the AFDW thickness is much smaller than the sample dimensions. In such cases the motion can be described with a reduced number of dynamical variables. The most natural way to introduce these variables is through the integral of motion for the moving AFDW in the absence of external forces. The integral of motion related to translation invariance is the momentum of the AFDW [see Eq. (6) in Ref. [34]]. Variation of momentum is due to the presence of external forces that break translational invariance of space (ponderomotive forces) and time inversion (dissipative and gyrotropic forces).

Following this derivation, the equation for the AFDW momentum is given by $P_x \propto -\int(\partial\theta/\partial x)\dot{\theta}dx$ [14], instead of the explicit Eq. (2) for the AFDW profile. Doing this, one obtains that for a steady moving texture, $P_x \propto v/\sqrt{1-v^2/c^2}$; i.e., the dynamics is Lorentz invariant [14,15]. The corresponding equation of motion takes the form

$$\frac{dP_x}{dt} = -\alpha_G \gamma H_{\mathrm{ex}} P_x + F_x, \tag{7}$$

where $F_x$ is the effective force that we specify below for each case. The detailed derivation of Eq. (7) is given in the Ref. [34], as are explicit expressions for external forces and the AFDW mass, $M_{\mathrm{AFDW}} \propto 1/H_{\mathrm{ex}}$. From Eq. (7) the relaxation time of the AFDW is given by $\tau_{\mathrm{AF}} = 1/\alpha_G \gamma H_{\mathrm{ex}}$. While both the mass and relaxation time are strongly suppressed in the AF due to exchange, the ratio $M_{\mathrm{AFDW}}/\tau_{\mathrm{AF}} = \alpha_G M_s S/\gamma x_{\mathrm{DW}}$ is independent of $H_{\mathrm{ex}}$ and is the same as in the FMDW (see Ref. [34]). This implies that the AFDW and FMDW mobilities below the Walker breakdown are comparable, as shown earlier in Eqs. (5) and (6).

Equation (7) shows the Lorentz invariant relativistic character of AF dynamics, where the width of the AFDW depends on its velocity; it shrinks by a factor $\sqrt{1-v^2/c^2}$.

To compare the effects of Néel and Zeeman fields, we consider the dynamics of the 90° AFDW. Both fields remove the degeneracy of the states $\mathbf{L}_1 \perp \mathbf{L}_2$ and thus could produce the effective force per area, $F_x = w(\mathbf{L}_1) - w(\mathbf{L}_2)$ [see also Figs. 1(c) and 1(d)]. The possible ranges of the fields are limited by the critical values at which one of the equilibrium states disappears: by the spin-flop field, $H_{\mathrm{sf}} = \sqrt{H_{\mathrm{an}} H_{\mathrm{ex}}}$, in the case of the Zeeman field, and by $H_{\mathrm{an}}$ in the case of the Néel field. If both fields are applied parallel to one of the easy axes [Figs. 1(c) and 1(d)], they can compete with or add to each other, depending on the sign of the Néel field (sign of the applied current), and from Eq. (7) the velocity of steady motion is

$$v^{\mathrm{AF}}_{\mathrm{steady}} = c\frac{B_{\mathrm{Neel}} - B^2_{\mathrm{Zee}}/(2H_{\mathrm{ex}})}{\sqrt{\alpha_G^2 H_{\mathrm{an}} H_{\mathrm{ex}} + [B_{\mathrm{Neel}} - B^2_{\mathrm{Zee}}/(2H_{\mathrm{ex}})]^2}}. \tag{8}$$

Figure 3 shows the field dependence of the velocity calculated from Eq. (3) (180° AFDW) and Eq. (8) (90° AFDW) for $Mn_2Au$ taking $H_{\mathrm{ex}} = 1307$ T [40], in-plane $H_{\mathrm{an}} = 0.03$ T [41], and setting $\alpha_G = 10^{-3}$.

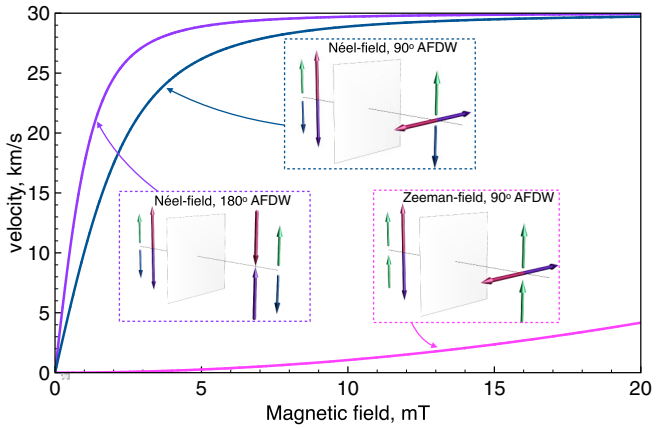


FIG. 3. Velocity of a 180° (violet line) and a 90° (green-blue line) AFDW vs an effective Néel field and a 90° AFDW (magenta line) vs a Zeeman field calculated for $Mn_2Au$ (we set AF magnon velocity $c = 30$ km/s).

The 3-orders-of-magnitude difference in the effective force occurs due to the exchange reduction of the Zeeman-field effects in an AF. As a result, the contribution of the Zeeman field to the domain wall velocity (magenta line in Fig. 3) is vanishingly small compared to the contribution of the Néel field (green-blue line). Experimentally, the effectiveness of the Néel field compared to the Zeeman field has been observed for current-induced reconfiguration of 90° rotated domains in AF CuMnAs [3]. From microscopic calculations of the Néel field in CuMnAs [3], the AF states were switched by currents corresponding to $B_{\mathrm{Neel}} \sim 1$ mT, while the Zeeman field up to 12 T was not sufficient for switching.

We also note that the maximum domain wall velocity observed up to now in the synthetic AFs was at current densities $3 \times 10^8$ A/cm$^2$ [20]. From our calculations, the same AFDW velocity in bulk AF $Mn_2Au$ corresponds to a staggered spin-orbit field of 0.07 mT, which corresponds to a current density of $3.5 \times 10^5$ A/cm$^2$ [3].

Another experimentally relevant calculation is the domain wall displacement driven by short pulses. In Fig. 4, a single rectangular pulse is delivered with a field magnitude corresponding to a steady-state domain wall velocity of 250 m/s (the maximum FMDW velocity reached in experiment [42]). For the AFDW we consider the Néel field, for the FMDW the Zeeman field, and the relaxation times for the AF and FM are $\tau_{\mathrm{AF}} = 1$ ps and $\tau_{\mathrm{FM}} = 1$ ns, respectively. Although the ultimate displacement of both the FMDW and the AFDW is the same, the AFDW attains it much faster due to its low mass and the resulting weak AFDW inertia. The favorable characteristics of AFDW dynamics compared to FMDW is more pronounced at short pulses ($\ll \tau_{\mathrm{FM}}$), as shown in Fig. 4.

The results presented here open a new way to manipulate AFDWs by electrical currents. This may enable future

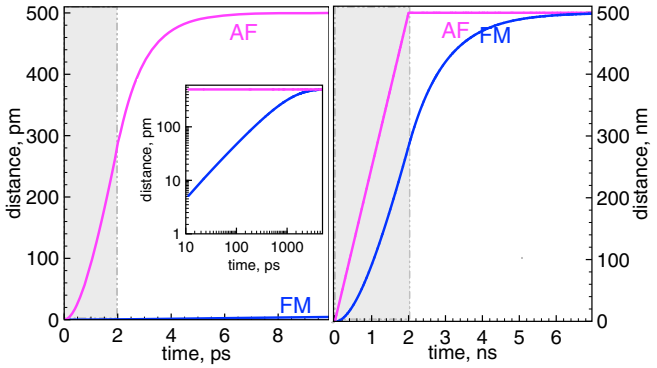


FIG. 4. Shift of (a) an AFDW (magenta lines) and (b) a FMDW (blue lines) under the action of a field pulse (duration of pulse shown as grey region). Field values in both cases correspond to the steady velocity of 250 m/s in the dc field. Relaxation times are $\tau_{AF} = 1$ ps and $\tau_{FM} = 1$ ns for AF and FM, respectively. In (a) the pulse duration $\tau = 2$ ps is much smaller than the relaxation time of FM ($\tau_{FM}$) but larger than $\tau_{AF}$. The inset shows the time dependence at large time scales. In (b) the pulse duration $\tau = 2$ ns is larger than $\tau_{FM} \gg \tau_{AF}$.

spintronic devices utilizing fast AFDW motion and serve as a practical tool for experimentally investigating spin dynamics of AF textures.

We acknowledge support from the Humboldt Foundation, from the Ministry of Education of the Czech Republic Grant No. LM2011026, and from the Grant Agency of the Czech Republic Grant No. 14-37427. We thank V. Amin for help with creating the graphics.

*Corresponding author.
helen.gomonay@gmail.com

[1] T. Jungwirth, X. Marti, P. Wadley, and J. Wunderlich, Nat. Nanotechnol. **11**, 231 (2016).
[2] Editorial, Nat. Nanotechnol. **11**, 205 (2016).
[3] P. Wadley *et al.*, Science **351**, 587 (2016).
[4] C. H. Marrows, Science **351**, 558 (2016).
[5] J. Železný, H. Gao, K. Výborný, J. Zemen, J. Mašek, A. Manchon, J. Wunderlich, J. Sinova, and T. Jungwirth, Phys. Rev. Lett. **113**, 157201 (2014).
[6] A. Y. Silov, P. A. Blajnov, J. H. Wolter, R. Hey, K. H. Ploog, and N. S. Averkiev, Appl. Phys. Lett. **85**, 5929 (2004).
[7] Y. K. Kato, R. C. Myers, A. C. Gossard, and D. D. Awschalom, Phys. Rev. Lett. **93**, 176601 (2004).
[8] S. D. Ganichev, S. N. Danilov, P. Schneider, V. V. Bel'kov, L. E. Golub, W. Wegscheider, D. Weiss, and W. Prettl, J. Magn. Magn. Mater. **300**, 127 (2006).
[9] J. Wunderlich, B. Kaestner, J. Sinova, and T. Jungwirth, Phys. Rev. Lett. **94**, 047204 (2005).
[10] A. Chernyshov, M. Overby, X. Liu, J. K. Furdyna, Y. Lyanda-Geller, and L. P. Rokhinson, Nat. Phys. **5**, 656 (2009).
[11] I. M. Miron *et al.*, Nat. Mater. **9**, 230 (2010).
[12] Note that the origin of the NSOT field is unrelated to a staggered field that would result from an alternating sign of the $g$ factor in the antiferromagnetic lattice.
[13] P. Wadley *et al.*, Sci. Rep. **5**, 17079 (2015).
[14] F. D. M. Haldane, Phys. Rev. Lett. **50**, 1153 (1983).
[15] A. Kosevich, B. Ivanov, and A. Kovalev, Phys. Rep. **194**, 117 (1990).
[16] S. K. Kim, Y. Tserkovnyak, and O. Tchernyshyov, Phys. Rev. B **90**, 104406 (2014).
[17] R. Wieser, E. Y. Vedmedenko, and R. Wiesendanger, Phys. Rev. Lett. **106**, 067204 (2011).
[18] K. M. D. Hals, Y. Tserkovnyak, and A. Brataas, Phys. Rev. Lett. **106**, 107206 (2011).
[19] H. Saarikoski, H. Kohno, C. H. Marrows, and G. Tatara, Phys. Rev. B **90**, 094411 (2014).
[20] S.-H. Yang, K.-S. Ryu, and S. Parkin, Nat. Nanotechnol. **10**, 221 (2015).
[21] E. G. Tveten, T. Müller, J. Linder, and A. Brataas, Phys. Rev. B **93**, 104408 (2016).
[22] I. V. Baryakhtar and B. A. Ivanov, Sov. J. Low Temp. Phys. **5**, 361 (1979).
[23] I. V. Bar'yakhtar and B. A. Ivanov, Solid State Commun. **34**, 545 (1980).
[24] A. F. Andreev and V. I. Marchenko, Sov. Phys. Uspekhi **23**, 21 (1980).
[25] S.-M. Seo, K.-W. Kim, J. Ryu, H.-W. Lee, and K.-J. Lee, Appl. Phys. Lett. **101**, 022405 (2012).
[26] N. L. Schryer and L. R. Walker, J. Appl. Phys. **45**, 5406 (1974).
[27] M. T. Hutchings and E. J. Samuelsen, Phys. Rev. B **6**, 3447 (1972).
[28] R. Cywinski, T. J. Hicks, S. J. Campbell, and P. Wells, Solid State Commun. **34**, 129 (1980).
[29] M. Wiltshire and M. Elcombe, Physica (Amsterdam) **120B +C**, 167 (1983).
[30] M. Wiltshire and M. Elcombe, J. Magn. Magn. Mater. **31–34**, 127 (1983).
[31] D. Welz, M. Kohgi, Y. Endoh, M. Nishi, and M. Arai, Phys. Rev. B **45**, 12319 (1992).
[32] G. S. D. Beach, C. Nistor, C. Knutson, M. Tsoi, and J. L. Erskine, Nat. Mater. **4**, 741 (2005).
[33] I. M. Miron *et al.*, Nat. Mater. **10**, 419 (2011).
[34] See Supplemental Material at http://link.aps.org/supplemental/10.1103/PhysRevLett.117.017202 for equations for energy-momentum of an antiferromagnetic texture, which includes Refs. [24,35–39].
[35] B. A. Ivanov and A. K. Kolezhuk, Low Temp. Phys. (Fiz. Nizk. Temp.) **21**, 275 (1995).
[36] H. V. Gomonay and V. M. Loktev, Phys. Rev. B **81**, 144427 (2010).
[37] H. V. Gomonay, R. V. Kunitsyn, and V. M. Loktev, Phys. Rev. B **85**, 134446 (2012).
[38] E. G. Tveten, A. Qaiumzadeh, O. A. Tretiakov, and A. Brataas, Phys. Rev. Lett. **110**, 127208 (2013).
[39] E. Schloemann, J. Appl. Phys. **43**, 3834 (1972).
[40] H. C. Wu, Z.-M. Liao, R. G. Sumesh Sofin, G. Feng, X.-M. Ma, A. B. Shick, O. N. Mryasov, and I. V. Shvets, Adv. Mater. **24**, 6374 (2012).
[41] A. B. Shick, S. Khmelevskyi, O. N. Mryasov, J. Wunderlich, and T. Jungwirth, Phys. Rev. B **81**, 212409 (2010).
[42] X. Jiang, L. Thomas, R. Moriya, M. Hayashi, B. Bergman, C. Rettner, and S. S. P. Parkin, Nat. Commun. **1**, 25 (2010).